VELOCITY MODEL UPDATE USING MIGRATION TO RESIDUAL TIME

Tilman Klüver

email: *tilman.kluever@gpi.uni-karlsruhe.de*

keywords: *tomography, migration, velocity model building*

ABSTRACT

The common-reflection-surface stack can be used to extract traveltime information for tomographic inversion schemes from seismic prestack data. The extracted information is a second order approximation. Thus, the obtained velocity models can only explain the prestack data up to second order.
In this paper I present a technique to update these models. The method makes use of residual traveltime information picked in CIG gathers and is, therefore, beyond second order. Migration is performed only for selected depth points and directly to residual time. The picking of residual moveout does not need to follow a specific trend, for example, a parabolic one. The inversion algorithm is demonstrated on a first synthetic data example.

INTRODUCTION

Many approaches to obtain accurate migration velocity models exist. Basically, these methods can be divided in two classes: One class works directly in the migrated domain like, e. g., focusing analysis and scanning approaches, and is based on iterative migration (Al-Yahya, 1989; MacKay and Abma, 1992). The other methods work in the time domain like classical traveltime tomography (Bishop et al., 1985; Farra and Madariaga, 1988). Some mixtures exist, for example, the time residuals for traveltime tomography may be picked and calculated in the depth migrated domain (Stork, 1992). All these methods suffer from several drawbacks. Picking in the prestack data along continuous events is very time-consuming and error-prone. Performing several depth migrations is also very time consuming.

To overcome these drawbacks new methods have been developed in the last years. They make use of the idea of a locally coherent event, either in the time or depth domain (Billette and Lambaré, 1998; Chauris et al., 2002). Thus, there is no longer a need to identify continuous reflection events. One further method of this type is CRS-based tomography (Duveneck, 2004) which I will call NIP-wave tomography as it uses the focusing of the normal incidence point (NIP) wave at zero traveltime as imaging condition. Instead of using only traveltime residuals also slope and curvature information is included into the tomographic inversion scheme. The method works completely in the poststack domain. Therefore, the identification of locally coherent events is notably easy and can be performed in a highly automated way (Klüver and Mann, 2005).

However, as only poststack quantities enter into NIP-wave tomography it is limited to the accuracy of these quantities. The input for NIP-wave tomography is usually obtained by means of the CRS stack (Mann et al., 1999) which uses a second-order traveltime approximation. Thus, the obtained model is limited to second order as well. This means that we will explain as good as possible our prestack data up to second order. As we will see later on in the data example this might not be enough to flatten our image gathers completely.

Nevertheless, NIP-wave tomography provides at least a very good initial model for a further update. In this paper I will present such an update technique. From a physical point of view it is based on the same principle as NIP-wave tomography: a smooth velocity model is searched for in which all diffraction

traveltime responses associated with the picks in the poststack time domain will focus in depth. In contrast to NIP-wave tomography the diffraction response is no longer approximated but is calculated accurately for each depth point. The curvature information is replaced by traveltime residuals picked in common image gathers (CIG) of small temporal extent. These CIGs are obtained by migrating directly to residual time, a concept I will explain later on. The advantage is that there is no need to perform a complete depth migration, the migration is performed only for selected depth points and, thus, only for these depth points the diffraction responses have to be calculated. Furthermore, CIGs in residual time show no pulse stretch.

First, I briefly review the concepts of Kirchhoff depth migration. Then, I will explain the concept of migration to residual time and I will compare residual moveout analyses in residual time with moveout analyses in depth. This will lead to the presentation of the new method. After a short comparison with NIP-wave tomography I will present the results of a first test on synthetic data. This test will clearly show that the sequence of NIP-wave tomography and the here presented updating technique can provide accurate velocity models for depth migration.

KIRCHHOFF MIGRATION AND VELOCITY ANALYSES

In standard Kirchhoff prestack depth migration the amplitude for a selected depth point M is obtained by a weighted summation along the Huygens surface in the time domain. The Huygens surface is given by all points N in the time domain for which the traveltime equals the sum of traveltimes from the source and from the receiver to a depth point M,

$$t = \tau_D(x_S, x_G|M) = \tau_D(x_S|M) + \tau_D(x_G|M)\ . \tag{1}$$

Mathematically, Kirchhoff migration corresponds to an integration of the recorded wavefield along the Huygens surface τ_D for each depth point M:

$$V(M) \propto \int_{x_1}^{x_2} \int_{h_1}^{h_2} dx_m\, d_h\, W(x_m, h|M)\, \partial_t^{1/2}\, U(x_m, h, t) \Big|_{t=\tau_D(x_m,h)}\ . \tag{2}$$

In above equation, U is the recorded wavefield, V denotes the migrated image, W is an optional migration weight and $\partial_t^{1/2}$ is a half-derivative in the time domain. Equation (2) is expressed in midpoint (x_m) and half-offset (h) coordinates as mostly used in practice. In this paper I assume the migration weight to be equal to one as I am only interested in kinematic features.

Using the correct migration velocity field yields a well-focused structural image of the subsurface. Omitting the summation in the offset domain, thus creating a separate migrated image for each offset, one can prove the correctness of the migration velocity field using the created common image gathers (CIG). One common image gather contains all traces for one lateral position, each trace with a different offset. For a correct velocity field , all events in a CIG are flat. A migration velocity too low yields upwards bending of the events (negative moveout), whereas a velocity too high results in downward bending (positive moveout). Measuring these moveouts in a number of selected CIGs forms the basis of various kinds of migration velocity analyses. The aim of all these methods is to flatten the CIGs.

Instead of using midpoint and half-offset coordinates, one can use the illumination angle ψ and the scattering angle θ as coordinates to formulate the Kirchhoff integral (Xu et al., 2001). In Figure 1 you find a graphical explanation of the two angles: The scattering angle is half of the opening angle between the incident and emerging ray. The illumination direction is the sum of the two slowness vectors of the incident and emrging ray. In the case of non-converted waves the illumination angle is the angle between the vertical and the bisecting line between the incident and emerging ray. Assuming the depth point belongs to a reflector, there exists one illumination angle which coincides with the reflector dip. This special angle will be referred to as ψ_0 later on. The source and receiver coordinates or midpoint and half-offset coordinates, respectively, are then a function of these two angles:

$$x_S = x_S(\theta, \psi) \qquad \text{and} \qquad x_G = x_G(\theta, \psi) \tag{3}$$

Inserting equation (3) into equation (2) yields the Kirchhoff integral in the angle domain

$$V(M) \propto \int_{\psi_1}^{\psi_2} \int_{\theta_1}^{\theta_2} d\psi\, d\theta\, W(\psi, \theta|M)\, \partial_t^{1/2}\, U(\psi, \theta, t) \Big|_{t=\tau_D(\psi,\theta)}\ . \tag{4}$$

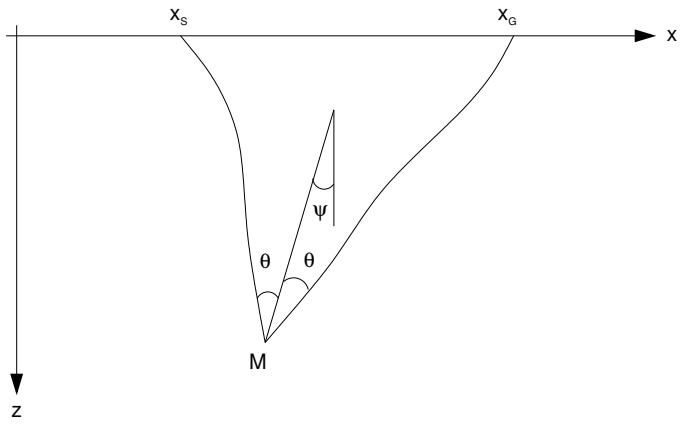

Figure 1: Explanation of illumination and scattering angle. See main text for details. Note that this definition of the illumination angle is valid for non-converted waves only.

Instead of performing a double summation over the midpoint and offset domain, now a summation over the illumination angle and scattering angle domain is carried out. Omitting the summation over the scattering angle, one obtains CIGs in the angle domain. These gathers can be used, as mentioned above, to measure the residual moveout and to perform a migration velocity analysis.

For the migration to be carried out, the Huygens surface τ_D has to be determined for every depth point M in the target zone.

MIGRATION TO RESIDUAL TIME

Let us assume we have determined the Huygens surface τ_D for a depth point M. To obtain the amplitude V(M) for this point we would carry out the double summation as indicated in equations (2) or (4). To determine the amplitude V of a neighboring sample on our output trace, we need to calculate the Huygens surface for this neighboring depth point. In this way, we can compute a common image gather around point M, where M is located on the migrated image for zero offset (or, alternatively, for zero scattering angle) of an actual reflector. Assuming at the point M a locally constant velocity, we can transform any residual moveout Δz from depth to residual traveltime Δt using

$$\Delta t = \frac{\Delta z}{v} \left(\cos(\psi_0 - \theta) + cos(\psi_0 + \theta)\right) . \tag{5}$$

In this case, ψ_0 is the reflector dip.

In a correct velocity model where we do not observe any residual moveout, our Huygens surface for point M corresponds to a surface of residual traveltime $\Delta t = 0$. This forms the basis of migration to residual time. Instead of having a depth dependence of the migrated image it is directly transformed to residual time. For neighboring samples of point M the Huygens surface is obtained by shifting the one associated with M by an amount δt, where δt is the sampling in residual time of the output traces. This output traces can be transformed back to residual depth using equation (5). Obviously, the length of the output trace is limited as I have assumed a locally constant velocity around point M.

Let me compare conventional migration with migration to residual time using a simple depth model. The model consists of one horizontal reflector located in a depth of 2000 m in a constant velocity medium with v = 2000 m/s. Both migrations have been carried out with the correct velocity model. The standard Kirchhoff migration produced an image gather in the Δz-offset-domain whereas the migration to residual time was carried out to produce an image gather in the Δt-θ-domain. The maximum offset of 3000 m used in the conventional migration corresponds to a reflection angle of approximately 36 degrees. As we can see in Figure 2, the migration to residual time shows no stretch with increasing scattering angle as observed in the standard migration result. The stretch occurs due to the angle dependent scaling factor between time and depth in equation (5) (Tygel et al., 1994). This means that no mute function has to be applied to

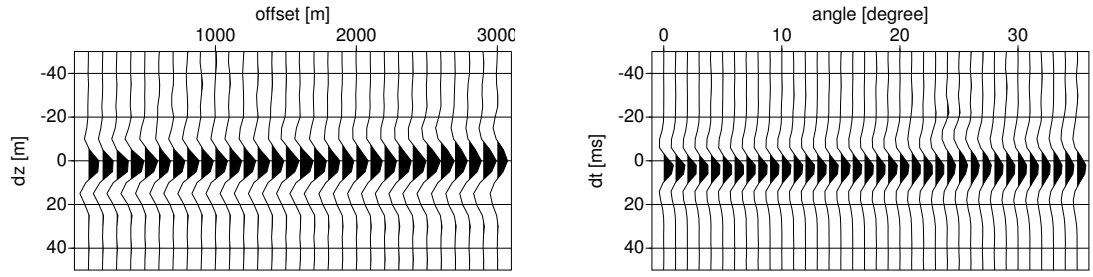

Figure 2: Common-image gathers in depth (left) and residual time (right) obtained using the correct migration velocity. Due to the angle dependent transformation between residual time and residual depth (see equation (5)) the image gather in the depth domain shows a wavelet stretch with increasing offset.

image gathers in residual time. Therefore, more traces may contribute to a residual moveout analysis. This especially holds for shallow events.

RESIDUAL MOVEOUT ANALYSES

The migration results in Figure 2 were obtained using the correct velocity model and knowing the correct reflector position. Let us now assume the reflector is located in a depth of 1960 m instead of the correct depth of 2000 m. Once again carrying out the two migrations using the correct velocity model we obtain the following results: In the conventional image gather we observe the reflector shifted to a depth residual $\Delta z = 40$ m as the image gather is centered around a depth of 1960 m. This depth residual remains constant for all offsets. The residual time along the zero-offset specular ray (two-way) is 40 ms. This is exactly the position where we observe our event in the residual time image gather at a scattering angle of zero degree. With increasing scattering angle we observe a decreasing residual time according to equation (5).

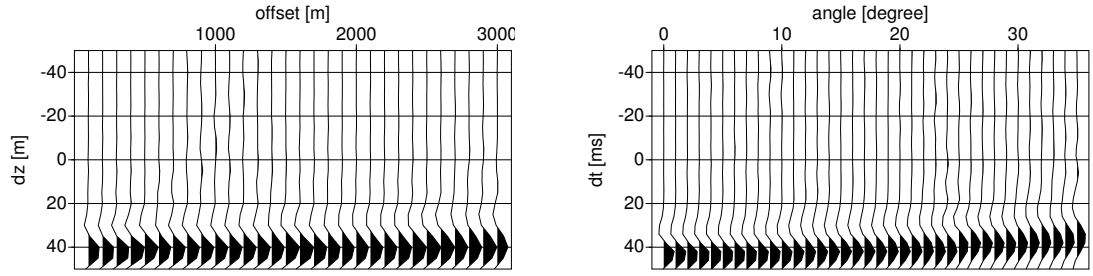

Figure 3: Image gathers obtained with conventional migration (left) and migration to residual time (right) using the correct velocity model. A wrong reflector depth of 1960 m/s was supposed.

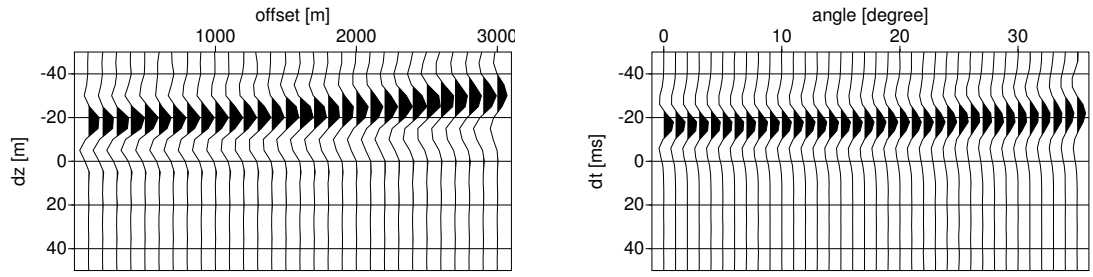

Figure 4: Image gathers obtained with conventional migration (left) and migration to residual time (right). A wrong migration velocity of 1980 m/s was used.

Now let us suppose, the reflector is positioned in a depth of 2000 m, i. e. in the correct depth, but let

us use a wrong migration velocity of 1980 m/s. We then obtain the image gathers shown in Figure 4. As expected we observe a ZO depth residual of 20 m which corresponds to a two-way time residual of approximately 20 ms. Because of the wrong migration velocity we observe an offset dependent residual depth Δz. Migration to residual time yields a corresponding time residual varying with the scattering angle θ. The relationship between depth residual Δz and residual time Δt is once again established by equation (5). The event is bended upwards because a too low migration velocity has been used. With a too high migration velocity we would observe the opposite behavior: Is the reflector located to deep by an amount Δz due to a too high migration velocity, i. e., $\Delta z > 0$, the traveltime along the specular ray is an amount Δt too high. The event in the CIG would be bended downwards in that case.

VELOCITY UPDATE USING MIGRATION TO RESIDUAL TIME

Picking the residual time in the image gathers for a number of depth points and various scattering angles these residuals can be used to perform a migration velocity update using residual traveltime tomography. In traveltime tomography the time residuals are inverted along the specular rays for a new position of the point M, a new reflector dip and, of course, for a change in the velocity model. This procedure is repeated until the traveltime residuals are sufficiently small. Usually, the points M are picked in the migrated image together with the reflector dip. For each of these points a residual moveout analysis is performed, the depth residuals are converted to time residuals using equation (5). These residuals are used to update the velocity model and the reflector geometry. For the next iteration a new prestack migration has to be carried out to pick the new and hopefully reduced depth residuals.This procedure requires to identify the reflectors in the depth domain and to introduce a mathematical description for them.

Here I will follow a different strategy: I want to use locally coherent events identified in the time domain in a simulated ZO section. This allows to drop the explicit reflector description as each locally coherent event from the time domain is associated with its own depth point M. For a geometrical explanation see Figure 5.

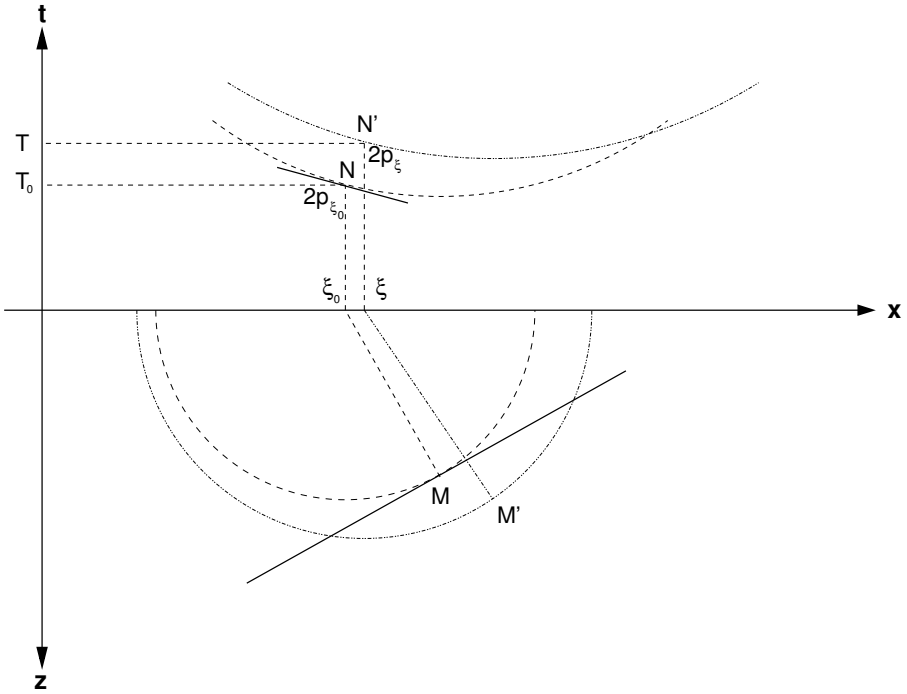

Figure 5: Link between time and depth domain. See main text for details.

In the time domain a locally coherent event at point N has been identified. This event is characterized by its lateral position ξ_0, its dip $2\,p_{\xi_0}$ and the ZO two way time (TWT) T_0. Performing a normal ray depth migration of point N with the ZO one way time (OWT) $t_0 = T_0/2$ using the correct velocity model maps N

to the correct depth point M. The initial direction of the normal ray (dashed) is directly related to the time dip of the locally coherent event. The locally coherent event in time might be part of a reflector in depth as illustrated here. The point M characterizes the point of tangency in depth between the isochron (dashed curve in depth) and the reflector. In time the point of tangency between the locally coherent event and the Huygens curve for ZO (dashed curve in time), the so-called stationary point, is given by N. Using the correct velocity model we will for each offset or scattering angle θ, respectively, map the energy summed up along the Huygens surface to point M. Thus, we would not observe any residual moveout in our CIG.

Let us now consider the case carrying out a migration for point M' in a wrong velocity model. Forward modeling the ZO TWT T, the time dip $2\,p_\xi$ and lateral position ξ of the stationary point associated with M', we see that they deviate from the ones we know from picking the locally coherent event in the time domain. Migrating with the wrong velocity model to residual time around the Huygens surface of M', we will observe residual moveout in our image gather.

The idea of the migration velocity model update presented in this paper is to minimize the misfit between the forward modeled stationary point and the picked one and to minimize the residual moveout in the image gather for point M'. The knowledge of the stationary point in time substitutes the necessity to pick reflectors in depth. Migration can be carried out to obtain an image gather directly in residual time. Thus, there is no limitation in picking residual moveout due to the application of a mute function. Migration is carried out only for selected depth points and the Huygens surface has to be determined only for these points.

The model consists of all depth points associated with the picked stationary points in time. For each depth point we have a location and dip: $(x, z, \psi_0)_i$, $i = 1, \ldots, n_{\text{picks}}$. The velocity model itself is described by two-dimensional B-splines (de Boor, 1978). This is the same model representation as used by Duveneck (2004) in NIP-wave tomography.

The initial model is updated iteratively using standard traveltime tomography complemented with the tomographic inversion for the stationary point. The inversion stops when a cost-function S has been minimized in the least-squares sense. The cost-function contains the sum off all squared misfits and, additionally, a regularization term minimizing the second derivatives of the velocity model:

$$\begin{aligned} S = \sum_{i=1}^{n_{\text{picks}}} \left[\sigma_t^{-2}(t_i - t_{0_i})^2 + \sigma_p^{-2}(p_{\xi_i} - p_{\xi_{0_i}})^2 + \sigma_\xi^{-2}(\xi_i - \xi_{0_i})^2 + \sum_{j=1}^{n_\theta} \sigma_{\Delta t}^{-2}(\Delta t_i(\theta_j))^2 \right] + \\ \iint \sum_{i=1}^{n_x} \sum_{j=1}^{n_z} \left[\epsilon_{xx} v_{ij} \frac{\partial^2 \beta_i(x)}{\partial x^2} \beta_j(z) + \epsilon_{zz} v_{ij} \beta_i(x) \frac{\partial^2 \beta_j(z)}{\partial z^2} + \epsilon v_{ij} \beta_i(x) \beta_j(z) \right] dx dz \ , \end{aligned} \tag{6}$$

where the different σ and ϵ are weighting factors for the various terms. The number of used B-spline nodes is given by n_x and n_z. Imposing a constraint on the model smoothness is a common approach to regularize the inverse problem (Lailly and Sinoquet, 1996).

PICKING OF RESIDUAL TRAVELTIME

In each iteration of the update the angle-dependent residual times $\Delta t(\theta)$ have to be picked in the image gathers. Most standard applications parameterize the residual moveout by a parabolic function. The curvature can then be determined by coherence analysis like in standard stacking velocity analyses. This is generally a very robust possibility. However, if the residual moveout deviates from the parabolic shape wrong results are obtained. Such a deviation is common in complex models and we will observe it in the data example below. Another complication arising is that the point where the energy after migration can be found is not known a-priori, because the image gather is not centered around that point (see, e. g., Figure 4). For both reasons, I propose a different picking strategy. Since the image gather is sampled in time steps and there occurs no stretch with increasing scattering angle I cross-correlate each trace in the image gather with a part of the ZO trace centered around the stationary point which has been picked in that ZO section. Picking the maximum in the cross-correlation directly gives the residual time. The result of this picking procedure for one CIG used in the data example below is displayed in Figure 6. On the left side you see the ZO trace centered around the pick location. On the right side you find the image gather in residual time for the corresponding depth point. This image gather has been obtained using the initial guess of the depth

point location and the initial migration velocity model. As the depth point is not located at its true position and the model is wrong we observe a quite complex moveout behavior. Fitting a parabolic curve to this image gather would clearly lead to wrong results.

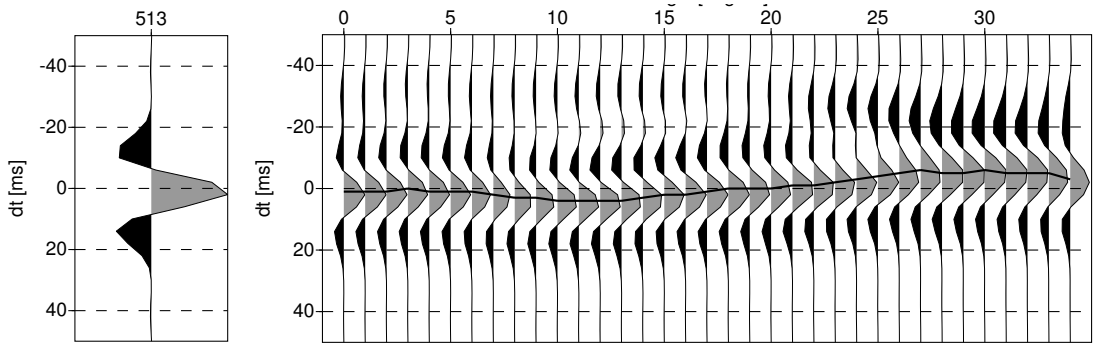

Figure 6: ZO trace and CIG for one pick. The ZO trace is centered around the picked TWT. A migration to residual time for the initial depth location of that pick using the initial velocity model yields the CIG shown on the ride side. Due to a wrong depth position and velocity model a quite complex moveout behavior can be observed. The picked moveout $\Delta t(\theta)$ is displayed by the curved black line.

COMPARISON WITH NIP-WAVE TOMOGRAPHY

In the data example below, I will use NIP-wave tomography to obtain the initial model for the above presented updating technique. Indeed, there exists a close connection between both methods as they are based on the same physical principle. Both methods try to find that position in depth and that velocity model which focuses the diffraction traveltime response for that point. Both methods make use of the connection between time and depth by a ZO normal ray. The main difference between both methods is that in NIP-wave tomography the diffraction response is approximated up to second order. This approximation can be extracted from the prestack data in a very robust manner but suffers from errors and will vary with the aperture chosen for the extraction. The method here overcomes this limitation as the diffraction response is exact in the current velocity model in each iteration. Thus, I am able to reduce residual moveout in the image gathers which is still observed after NIP-wave tomography due to its limitation to second order. However, the ZO time and the dip in the ZO section are determined after having performed a CMP stack. Thus, these quantities depend to some extent on the aperture chosen in the determination of the NMO velocity. In this respect, the here presented updating technique still remains second order.

DATA EXAMPLE

I have tested the above described updating technique on a synthetic data set. The model to for forward model the prestack data is shown in Figure 7. No noise was added to the data. The midpoints cover the range from -3960 m to 10000 m with a spacing of 15 m. Offsets up to 3960 m were simulated, the time sampling is 4 ms.

First, I applied the CRS stack to the data to obtain a simulated ZO section (Figure 8). Automatically, about 700 picks were selected in the stack section. These picks were used to perform NIP-wave tomography. The final inversion result can be seen in Figure 9.

The final model obtained by NIP-wave tomography served as initial model for the migration velocity model update. As initial depth locations, I took the final NIP-locations of the NIP-wave tomography. After four iterations of the update, I obtained the model shown in Figure 10. Compared to the result of NIP-wave tomography it shows much more details. Generally, it seems to be much closer to the original model as a comparison between Figure 7 and 10 reveals.

This becomes even clearer considering the obtained depth positions of the picks. In Figure 11 you find the dip bars for each obtained depth point after NIP-wave tomography plotted into the original model. The same plot is shown in Figure 12 for the dip bars after the model update. As you can see, especially in the

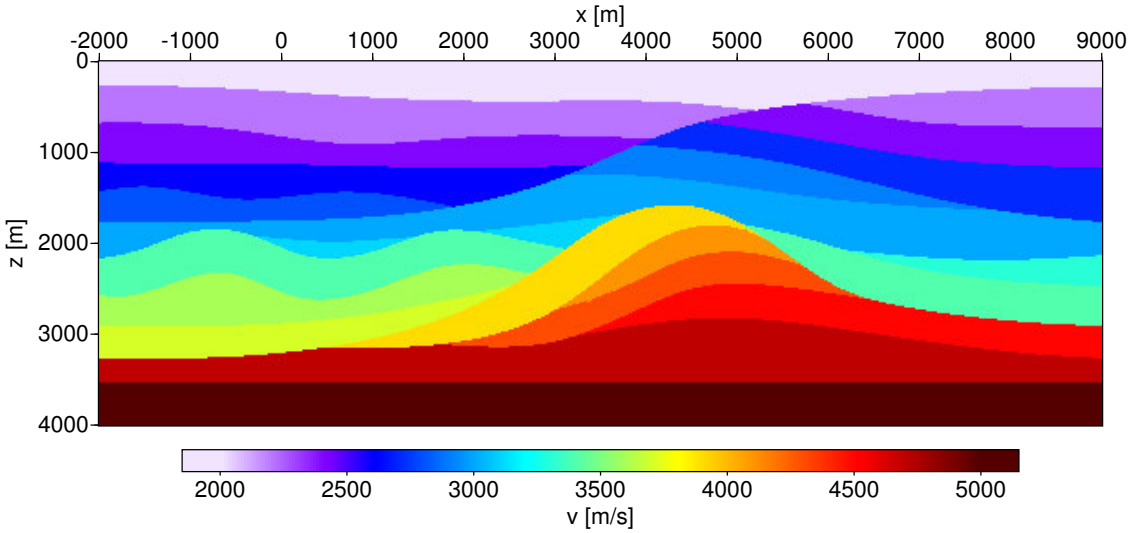

Figure 7: Model used for forward modeling of the synthetic data set.

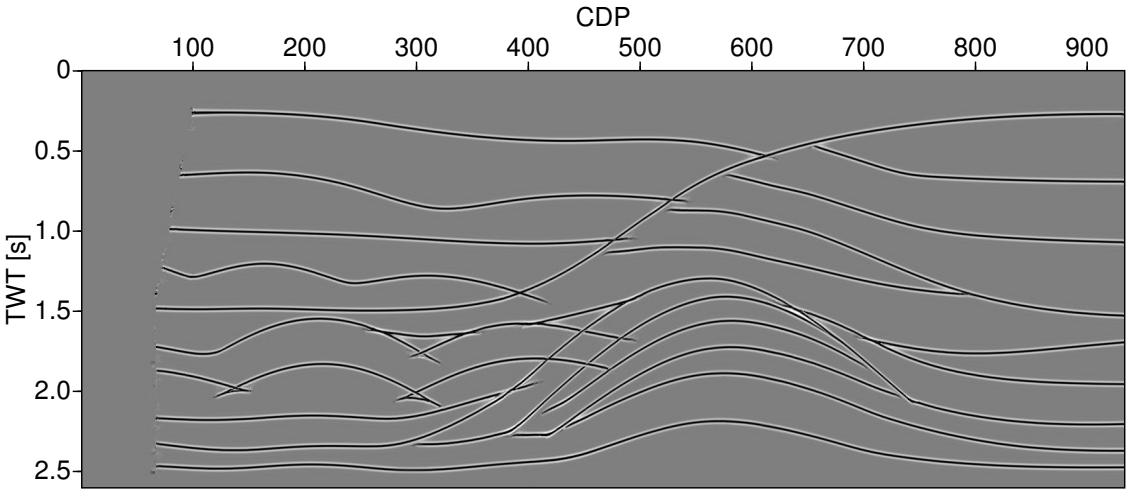

Figure 8: CRS stack section obtained for the synthetic data set. This section served for picking the input for NIP-wave tomography.

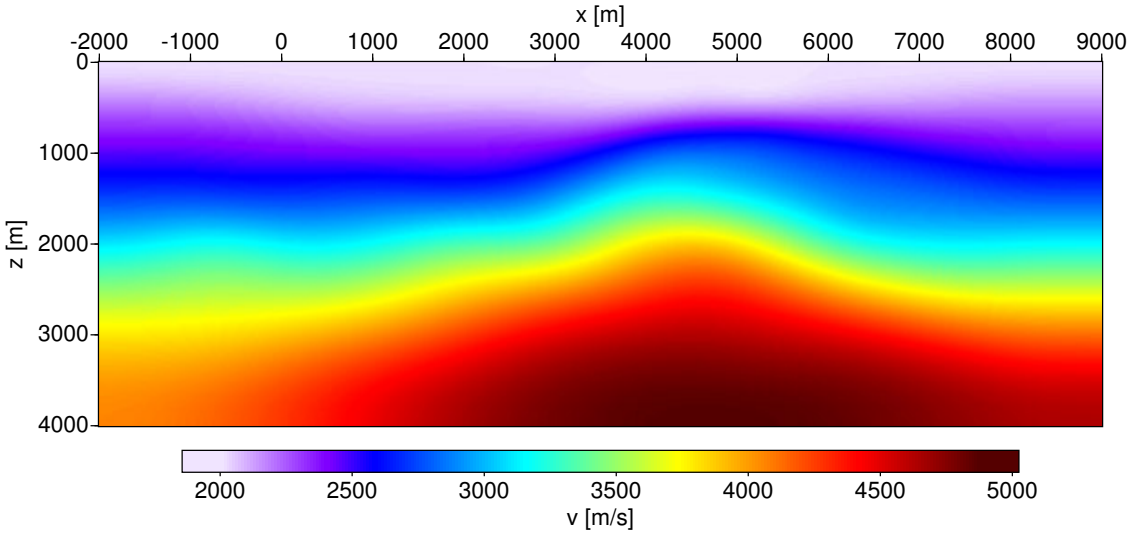

Figure 9: Inversion result after twelve iterations of NIP-wave tomography. This model shows the main features of the original model. However, we can not see much details.

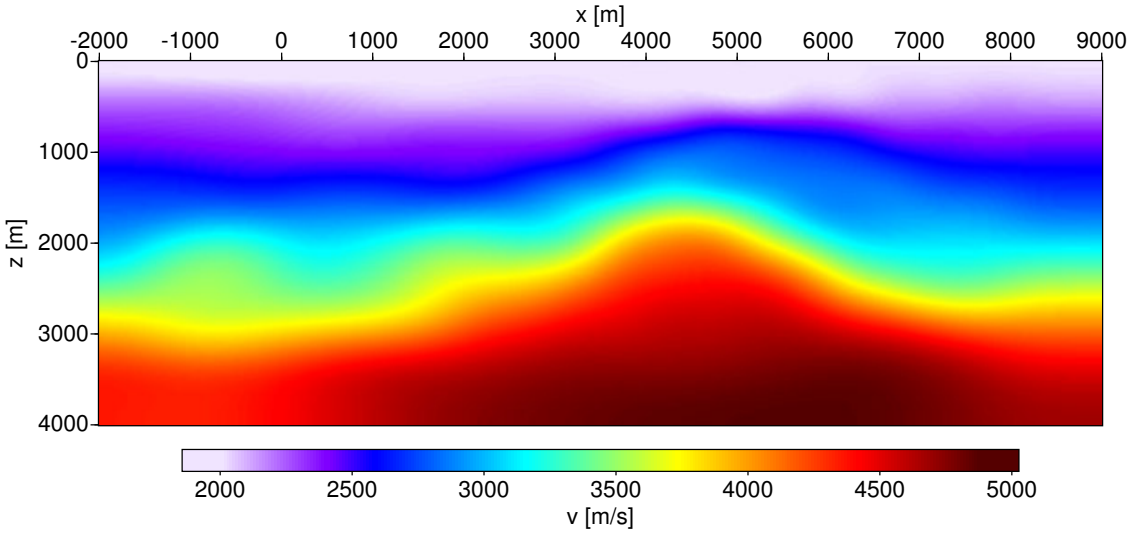

Figure 10: Inversion result after four iterations of residual traveltime tomography. Compared to the result of NIP-wave tomography (Figure 9) much more details of the original model (Figure 7) are resolved.

boxed regions, the dip bars after the update fit better the actual reflectors than after NIP-wave tomography alone.

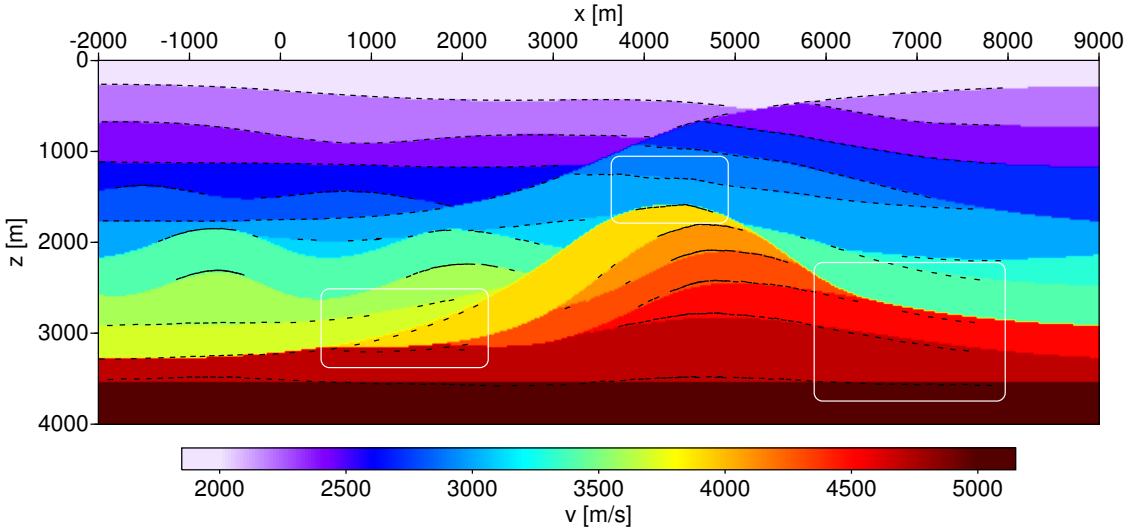

Figure 11: Original model with dip bars for depth points obtained by NIP-wave tomography. Note the quite large deviation of the inverted depth positions from the actual reflector locations.

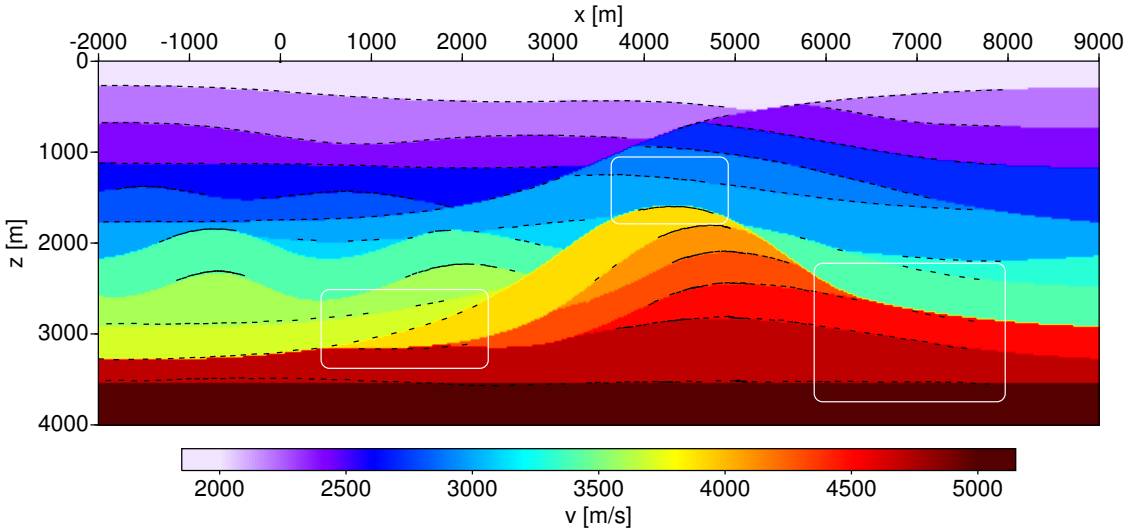

Figure 12: Original model with dip bars after velocity model update. Note the improved accordance between inverted and actual depths.

The final quality control for the obtained model after the update is to have a look at the CIGs. First, lets have a look at the CIG in residual time for the same pick as displayed in Figure 6 but now migrated with the updated velocity model and updated depth position. This CIG you find in Figure 13 together with the picked moveout. The moveout is significantly reduced after the update. This is more obvious comparing a number of conventional CIGs obtained for the final model of NIP-wave tomography and after the update. Therefore, I produced one CIG every 500 m between -500 m and 7000 m. The sets of image gathers for both models are displayed in Figure 14. The comparison shows that the overall moveout has been largely reduced after performing the model update which clearly demonstrates the success of the presented technique.

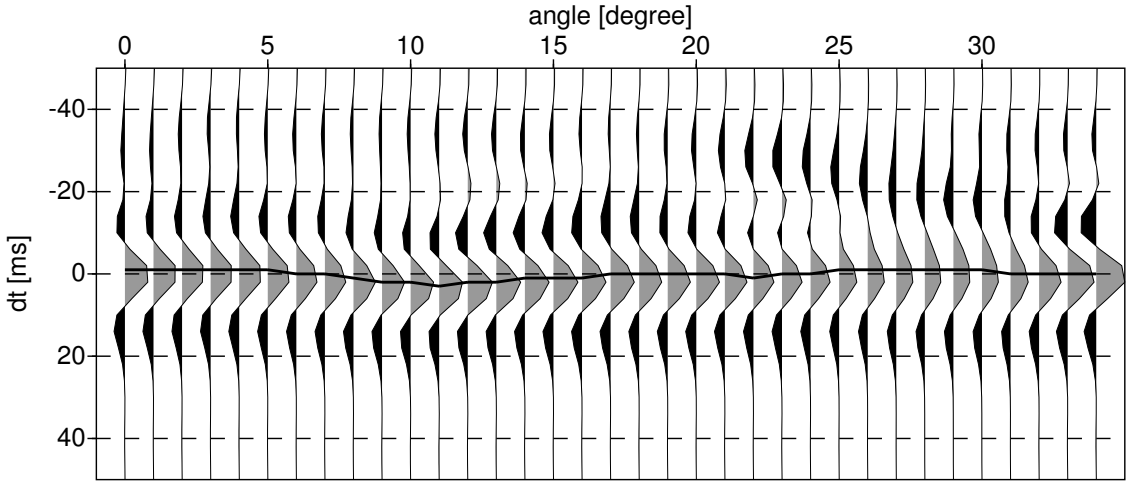

Figure 13: CIG in residual time for the same pick as in Figure 6 obtained with the updated velocity model. Compared to Figure 6 the residual moveout has been largely reduced. The picked moveout is indicated by the curved black line.

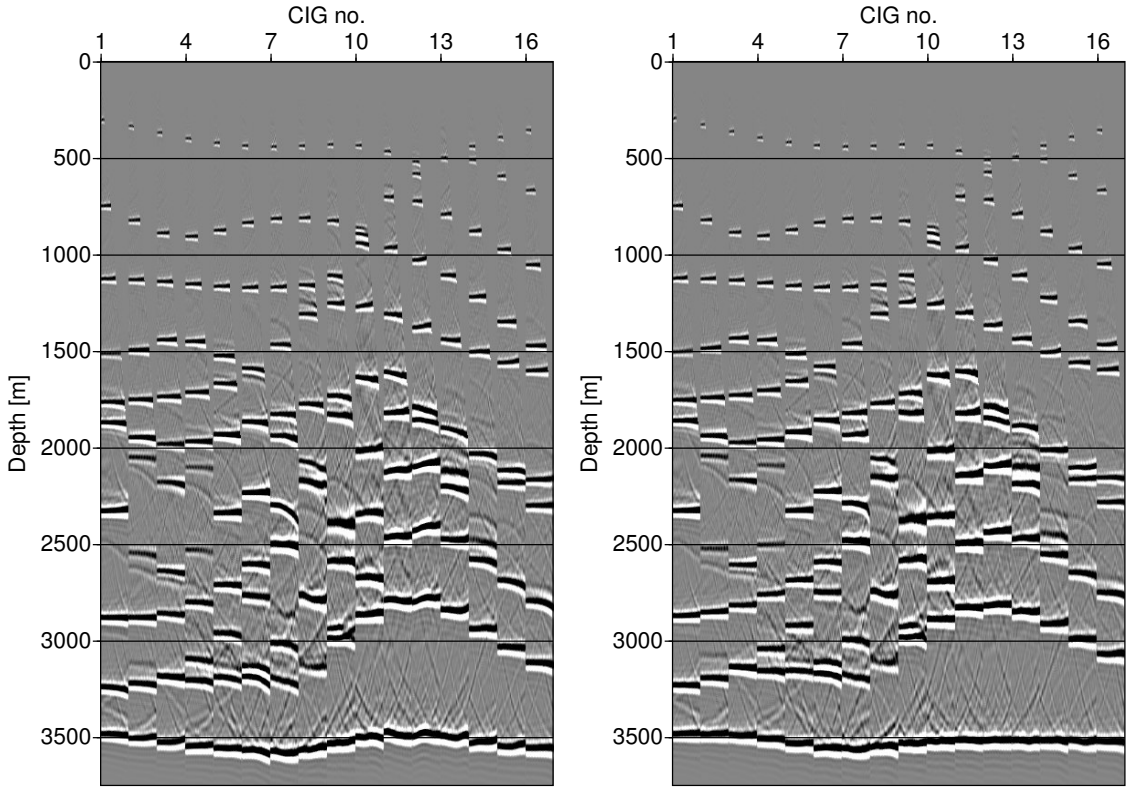

Figure 14: Comparison of CIGs between -500 m and 7000 m with a spacing of 500 m. On the left side the image gathers obtained after NIP-wave tomography, on the ride side the ones obtained with the updated velocity model. Note the generally improved flatness after the model update.

CONCLUSIONS

I have presented a new updating technique which provides accurate velocity models for depth migration. It is based on the same physical principles and model representation than NIP-wave tomography and is, thus, the ideal successor of that method in a processing chain. It partially overcomes the limitation to second order which is inherent in NIP-wave tomography.

The initial model of the presented method is obtained by NIP-wave tomography which is fast and robust as it works completely in the poststack domain with the concept of locally coherent events. This concept is retained in the new method as migration is performed only for a limited number of depth points directly to residual time. The presented picking technique for the residual moveout is able to handle moveout curves of any form. There is no parabolic representation as in most methods. A first test on a synthetic data example shows the potential of the new method. However, further tests on synthetic and real data are required.

ACKNOWLEDGMENTS

This work was kindly supported by the sponsors of the *Wave Inversion Technology (WIT) Consortium*, Karlsruhe, Germany.

REFERENCES

Al-Yahya, K. (1989). Velocity analysis by iterative profile migration. *Geophysics*, 54(6):718–729.

Billette, F. and Lambaré, G. (1998). Velocity macro-model estimation from seismic reflection data by stereotomography. *Geophys. J. Intern.*, 135:671–690.

Bishop, T., Bube, K., Cutler, R., Langan, R., Love, P., Resnick, J., Shuey, R., Spindler, D., and Wyld, H. (1985). Tomographic determination of velocity and depth in laterally varying media. *Geophysics*, 50(1):903–923.

Chauris, H., Noble, M., Lambaré, G., and Podvin, P. (2002). Migration velocity analysis from locally coherent events in 2-D laterally heterogeneous media, part I: theoretical aspects. *Geophysics*, 67(4):1202–1212.

de Boor, C. (1978). *A practical guide to splines*. Springer-Verlag, Berlin.

Duveneck, E. (2004). Velocity model estimation with data-derived wavefront attributes. *Geophysics*, 69(1):265–274.

Farra, V. and Madariaga, R. (1988). Non-linear reflection tomography. *Geophys. J.*, 95:135–147.

Klüver, T. and Mann, J. (2005). Smoothing and automated picking of kinematic wavefield attributes. In *Expanded abstracts, 75nd Ann. Internat. Mtg.* Soc. Expl. Geophys.

Lailly, P. and Sinoquet, D. (1996). Smooth velocity models in reflection tomography for imaging complex geological structures. *Geophys. J. Intern.*, 124:349–362.

MacKay, S. and Abma, R. (1992). Imaging and velocity estimation with depth-focusing analysis. *Geophysics*, 57(12):1608–1622.

Mann, J., Jäger, R., Müller, T., Höcht, G., and Hubral, P. (1999). Common-Reflection-Surface stack – a real data example. *J. Appl. Geoph.*, 42(3,4):301–318.

Stork, C. (1992). Reflection tomography in the postmigrated domain. *Geophysics*, 57(5):680–692.

Tygel, M., Schleicher, J., and Hubral, P. (1994). Pulse distortion in depth migration. *Geophysics*, 59(10):1561–1569. Discussion in GEO-60-6-1942-1949.

Xu, S., Chauris, H., Lambare, G., and Noble, M. (2001). Common-angle-migration: A strategy for imaging complex media. *Geophysics*, 66(6):1877–1894.